Meccanica (2016) 51:1913–1929
DOI 10.1007/s11012-015-0347-1

Sampling surfaces formulation for thermoelastic analysis of laminated functionally graded shells

G. M. Kulikov · S. V. Plotnikova ·
A. A. Mamontov

Received: 2 August 2015 / Accepted: 10 December 2015 / Published online: 21 December 2015

Abstract This paper focuses on implementation of the sampling surfaces (SaS) method for the three-dimensional (3D) thermal stress analysis of steady-state thermoelasticity problems for laminated functionally graded (FG) shells. The SaS formulation is based on choosing inside the *n*th layer I_n not equally spaced SaS parallel to the middle surface of the shell in order to introduce the temperatures and displacements of these surfaces as basic shell variables. Such choice of unknowns permits the presentation of the proposed thermoelastic FG shell formulation in a very compact form. The SaS are located inside each layer at Chebyshev polynomial nodes that improves the convergence of the SaS method significantly. As a result, the SaS formulation can be applied efficiently to analytical solutions for laminated FG shells, which asymptotically approach the 3D exact solutions of thermoelasticity as the number of SaS I_n tends to infinity.

G. M. Kulikov (✉) · S. V. Plotnikova · A. A. Mamontov
Department of Applied Mathematics and Mechanics,
Tambov State Technical University, Sovetskaya, 106,
Tambov, Russia 392000
e-mail: gmkulikov@mail.ru

S. V. Plotnikova
e-mail: plotnikovasvetlana62@gmail.com

A. A. Mamontov
e-mail: aamamontov87@mail.ru

Keywords Thermoelasticity · Functionally graded shell · 3D stress analysis · Sampling surfaces method

1 Introduction

Nowadays, the functionally graded (FG) materials are widely used in mechanical engineering due to their advantages compared to traditional laminated materials [5]. The study of FG materials is not a simple task because the material properties depend on the spatial coordinate and some specific assumptions regarding their continuous variations in the thickness direction are required [17]. This fact restricts the implementation of the Pagano approach [35, 49] for the 3D exact solutions of FG rectangular plates. However, this restriction can be overcome and even extend to cylindrical shells in the case of artificial dividing the shell into a large number of individual layers with constant material properties through the layer thickness [42]. Apparently, the use of such a technique means that 3D analytical solutions derived are approximate (see, e.g. [51]). The other popular approaches to 3D exact solutions are the state space approach [8] and the asymptotic approach [12]. Both of them were applied efficiently to FG plates and cylindrical panels subjected to thermomechanical loading [1–3, 11, 39, 43]. A new approach to closed-form elasticity solutions for FG isotropic and transversely isotropic plates is considered in papers [18, 50]. These solutions are based on the general solution of the equilibrium equations of inhomogeneous elastic media [37]. The efficient approach to the exact analysis of thermoelasticity was proposed in contributions [36, 46–48]. The authors studied the static and transient thermoelastic problems for FG simply supported plates and cylindrical panels with the material properties presented by Taylor series expansions through the thickness coordinate. The analytical solutions of elasticity for the transient thermoelastic response of FG strips and rectangular plates with simply supported edges under nonuniform heating on outer surfaces were obtained in works [32–34]. The closed-form solution for the FG cylindrical shell under temperature loading was derived in [16].

The sampling surfaces (SaS) formulation was proposed first for the 3D elasticity analysis of homogeneous and laminated shells in [22–24]. Further, it was extended to heat conduction analysis [25] and thermoelastic/thermoelectroelastic analysis [26, 27, 29] of laminated plates and shells. Recently, the SaS formulation has been applied to 3D thermoelastic analyses of FG plates [28]. However, the SaS approach has not been applied to 3D steady-state thermoelasticity problems for laminated FG shells including the metal/ceramic shells yet.

According to the SaS concept, we choose any surfaces inside the nth layer of the shell $\Omega^{(n)1}$, $\Omega^{(n)2}, \ldots, \Omega^{(n)I_n}$ parallel to the middle surface in order to introduce temperatures $T^{(n)1}, T^{(n)2}, \ldots, T^{(n)I_n}$ and displacement vectors $\mathbf{u}^{(n)1}, \mathbf{u}^{(n)2}, \ldots, \mathbf{u}^{(n)I_n}$ of these surfaces as basic shell variables, where I_n is the total number of SaS of the nth layer ($I_n \geq 3$). Such choice of temperatures and displacements with the consequent use of the Lagrange polynomials of degree $I_n - 1$ in the thickness direction for each layer allows one to present the governing equations of the thermoelastic laminated FG shell formulation in a very compact form.

It should be noted that the SaS formulation with equally spaced SaS does not work properly with the Lagrange polynomials of high degree because of Runge's phenomenon [41]. This phenomenon can yield the wild oscillation at the edges of the interval when the user deals with any specific functions that are appeared in a shell theory due to utilizing the curvilinear coordinates of the middle surface. If the number of equispaced nodes is increased then the oscillations become even larger. However, the use of the Chebyshev polynomial nodes (see, e.g. [9]) inside each layer can help to improve significantly the behavior of the Lagrange polynomials of high degree because such choice permits to minimize uniformly the error due to the Lagrange interpolation. This fact gives in turn an opportunity to derive the analytical solutions for laminated FG shells with a prescribed accuracy employing the sufficient number of SaS. Actually, it means that the analytical solutions based on the SaS formulation *asymptotically* approach the 3D exact solutions of thermoelasticity as the number of SaS $I_n \to \infty$.

The origins of the SaS concept can be found in contributions [20, 21] where three, four and five equally spaced SaS are employed. The SaS formulation with the arbitrary number of equispaced SaS is considered by the authors [22]. The more general approach with the SaS located at the Chebyshev polynomial nodes was developed later [23, 24]. Note also that the thermal stress analysis of laminated composite shells on the basis of Carrera's higher-order layer-wise formulation [10] can be found in many papers (see, e.g. [6, 7]). The doubly-curved shell formulation through the higher-order equivalent single layer theory [10] accounting for thickness stretching has been proposed in [44, 45]. Both free vibration and static problems are discussed with a particular emphasis on the stress recovery procedure. The authors report that their procedure leads to stable, accurate and reliable results for the moderately thick and thin doubly-curved shells with variable principal curvatures. However, for the analysis of thick doubly-curved shells instead of the post-processing stress recovery technique a more general approach based on the 3D constitutive equations should be applied. Such a question is discussed here in detail.

The authors restrict themselves to finding five *right* digits in all examples presented. To achieve a better accuracy, the more number of SaS for each layer should be taken.

2 Description of temperature and temperature gradient fields

Consider a thick laminated shell of the thickness h. Let the middle surface Ω be described by orthogonal curvilinear coordinates θ_1 and θ_2, which are referred to the lines of principal curvatures of its surface. The coordinate θ_3 is oriented along the unit vector $\mathbf{e}_3(\theta_1, \theta_2)$ normal to the middle surface. Introduce the following notations: $\mathbf{e}_\alpha(\theta_1, \theta_2)$ are the orthonormal base vectors of the middle surface; $A_\alpha(\theta_1, \theta_2)$ are the coefficients of the first fundamental form; $k_\alpha(\theta_1, \theta_2)$ are the principal curvatures of the middle surface; $c_\alpha = 1 + k_\alpha\theta_3$ are the components of the shifter tensor; $c_\alpha^{(n)i_n}(\theta_1, \theta_2)$ are the components of the shifter tensor at SaS defined as

$$c_\alpha^{(n)i_n} = c_\alpha(\theta_3^{(n)i_n}) = 1 + k_\alpha\theta_3^{(n)i_n}, \tag{1}$$

where $\theta_3^{(n)i_n}$ are the transverse coordinates of SaS inside the nth layer given by

$$\theta_3^{(n)1} = \theta_3^{[n-1]}, \quad \theta_3^{(n)I_n} = \theta_3^{[n]},$$
$$\theta_3^{(n)m_n} = \frac{1}{2}\left(\theta_3^{[n-1]} + \theta_3^{[n]}\right) - \frac{1}{2}h^{(n)}\cos\left(\pi\frac{2m_n - 3}{2(I_n - 2)}\right), \tag{2}$$

where $\theta_3^{[n-1]}$ and $\theta_3^{[n]}$ are the transverse coordinates of layer interfaces $\Omega^{[n-1]}$ and $\Omega^{[n]}$ depicted in Fig. 1; $h^{(n)} = \theta_3^{[n]} - \theta_3^{[n-1]}$ is the thickness of the nth layer.

Here and in the following developments, the index n identifies the belonging of any quantity to the nth layer and runs from 1 to N, where N is the number of layers; the index m_n identifies the belonging of any quantity to the inner SaS of the nth layer and runs from 2 to $I_n - 1$, whereas the indices i_n, j_n, k_n describe all SaS of the nth layer and run from 1 to I_n; Latin tensorial indices i, j, k, l range from 1 to 3; Greek indices α, β range from 1 to 2.

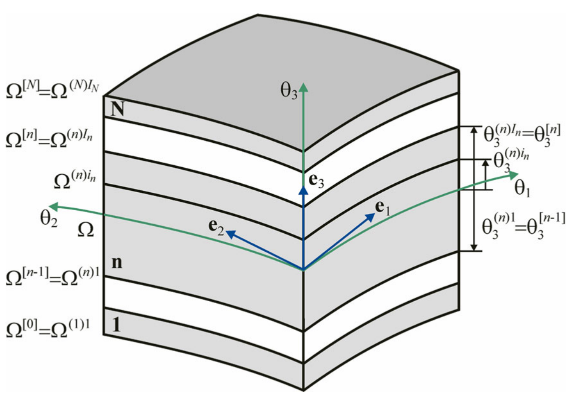

Fig. 1 Geometry of the laminated shell

Remark 1 It is seen from Eq. (2) that the transverse coordinates of inner SaS $\theta_3^{(n)m_n}$ coincide with coordinates of the Chebyshev polynomial nodes [9]. This fact has a great meaning for a convergence of the SaS method [23, 24].

The relation between the temperature T and the temperature gradient $\mathbf{\Gamma}$ is given by

$$\mathbf{\Gamma} = \nabla\mathbf{T}. \tag{3}$$

In a component form, it can be written as

$$\Gamma_\alpha = \frac{1}{A_\alpha c_\alpha}T_{,\alpha}, \quad \Gamma_3 = T_{,3}, \tag{4}$$

where the symbol $(\ldots)_{,i}$ stands for the partial derivatives with respect to coordinates θ_i.

We start now with the first and second assumptions of the proposed thermoelastic laminated shell formulation. Let us assume that the temperature and temperature gradient fields are distributed through the thickness of the nth layer as follows:

$$T^{(n)} = \sum_{i_n} L^{(n)i_n}T^{(n)i_n}, \quad \theta_3^{[n-1]} \le \theta_3 \le \theta_3^{[n]}, \tag{5}$$

$$\Gamma_i^{(n)} = \sum_{i_n} L^{(n)i_n}\Gamma_i^{(n)i_n}, \quad \theta_3^{[n-1]} \le \theta_3 \le \theta_3^{[n]}, \tag{6}$$

where $T^{(n)i_n}(\theta_1, \theta_2)$ are the temperatures of SaS of the nth layer $\Omega^{(n)i_n}$; $\Gamma_i^{(n)i_n}(\theta_1, \theta_2)$ are the components of the temperature gradient at the same SaS; $L^{(n)i_n}(\theta_3)$ are the Lagrange polynomials of degree $I_n - 1$ defined as

$$T^{(n)i_n} = T(\theta_3^{(n)i_n}), \tag{7}$$

$$\Gamma_i^{(n)i_n} = \Gamma_i(\theta_3^{(n)i_n}), \tag{8}$$

$$L^{(n)i_n} = \prod_{j_n \ne i_n} \frac{\theta_3 - \theta_3^{(n)j_n}}{\theta_3^{(n)i_n} - \theta_3^{(n)j_n}}. \tag{9}$$

The use of Eqs. (4), (5), (7) and (8) yields

$$\Gamma_\alpha^{(n)i_n} = \frac{1}{A_\alpha c_\alpha^{(n)i_n}}T_{,\alpha}^{(n)i_n}, \tag{10}$$

$$\Gamma_3^{(n)i_n} = \sum_{j_n} M^{(n)j_n}(\theta_3^{(n)i_n})T^{(n)j_n}, \tag{11}$$

where $M^{(n)j_n} = L_{,3}^{(n)j_n}$ are the derivatives of the Lagrange polynomials, which are calculated at SaS as follows:

$$M^{(n)j_n}\left(\theta_3^{(n)i_n}\right) = \frac{1}{\theta_3^{(n)j_n} - \theta_3^{(n)i_n}} \prod_{k_n \neq i_n, j_n} \frac{\theta_3^{(n)i_n} - \theta_3^{(n)k_n}}{\theta_3^{(n)j_n} - \theta_3^{(n)k_n}} \quad \text{for} \quad j_n \neq i_n,$$

$$M^{(n)i_n}\left(\theta_3^{(n)i_n}\right) = -\sum_{j_n \neq i_n} M^{(n)j_n}\left(\theta_3^{(n)i_n}\right). \tag{12}$$

It is seen from Eq. (11) that the transverse components of the temperature gradient on SaS of the nth layer $\Gamma_3^{(n)i_n}$ are represented as a linear combination of temperatures of SaS $T^{(n)j_n}$ of the same layer.

3 Description of displacement and strain fields

A position vector of the shell is written as $\mathbf{R} = \mathbf{r} + \theta_3\mathbf{e}_3$, where $\mathbf{r} = \mathbf{r}(\theta_1, \theta_2)$ is the position vector of any point of the middle surface. The base vectors in the shell body are given by

$$\mathbf{g}_\alpha = \mathbf{R}_{,\alpha} = A_\alpha c_\alpha \mathbf{e}_\alpha, \quad \mathbf{g}_3 = \mathbf{R}_{,3} = \mathbf{e}_3. \tag{13}$$

The position vector of the deformed shell is defined as

$$\bar{\mathbf{R}} = \mathbf{R} + \mathbf{u}, \tag{14}$$

where $\mathbf{u}$ is the displacement vector, which is measured in accordance with the total Lagrangian formulation from the initial configuration to the current configuration directly. The base vectors in the current shell configuration are written as

$$\bar{\mathbf{g}}_i = \bar{\mathbf{R}}_{,i} = \mathbf{g}_i + \mathbf{u}_{,i}. \tag{15}$$

Next, we represent the displacement vector in an orthonormal basis $\mathbf{e}_i$ as follows:

$$\mathbf{u} = u_i\mathbf{e}_i. \tag{16}$$

Here and in the following developments, the summation on repeated Latin indices is implied. Using Eq. (16) and well-known formulas for the derivatives of orthonormal base vectors $\mathbf{e}_i$ with respect to curvilinear coordinates θ_α [24], one obtains

$$\frac{1}{A_\alpha}\mathbf{u}_{,\alpha} = \lambda_{i\alpha}\mathbf{e}_i, \tag{17}$$

where $\lambda_{i\alpha}$ are the strain parameters expressed in terms of displacements as

$$\lambda_{\alpha\alpha} = \frac{1}{A_\alpha}u_{\alpha,\alpha} + B_\alpha u_\beta + k_\alpha u_3 \quad \text{for} \quad \beta \neq \alpha,$$

$$\lambda_{\beta\alpha} = \frac{1}{A_\alpha}u_{\beta,\alpha} - B_\alpha u_\alpha \quad \text{for} \quad \beta \neq \alpha,$$

$$\lambda_{3\alpha} = \frac{1}{A_\alpha}u_{3,\alpha} - k_\alpha u_\alpha, \quad B_\alpha = \frac{1}{A_\alpha A_\beta}A_{\alpha,\beta} \quad \text{for} \quad \beta \neq \alpha. \tag{18}$$

The Green–Lagrange strain tensor in an orthogonal curvilinear coordinate system [24] can be written as

$$2\varepsilon_{ij} = \frac{1}{A_iA_jc_ic_j}(\bar{\mathbf{g}}_i \cdot \bar{\mathbf{g}}_j - \mathbf{g}_i \cdot \mathbf{g}_j), \tag{19}$$

where one should set $A_3 = 1$ and $c_3 = 1$. Substituting base vectors (13) and (15) into the strain–displacement relationships (19), taking into consideration (17) and discarding non-linear terms, we arrive at the component form of these relationships

$$2\varepsilon_{\alpha\beta} = \frac{1}{c_\beta}\lambda_{\alpha\beta} + \frac{1}{c_\alpha}\lambda_{\beta\alpha},$$

$$2\varepsilon_{\alpha3} = \frac{1}{c_\alpha}\lambda_{3\alpha} + u_{\alpha,3}, \quad \varepsilon_{33} = u_{3,3}. \tag{20}$$

The following step consists in a choice of the suitable approximation of displacements and strains through the thickness of the nth layer. It is apparent that displacement and strain distributions should be chosen similar to temperature and temperature gradient distributions (5) and (6). Thus, the third and fourth assumptions of the proposed thermoelastic laminated FG shell formulation are

$$u_i^{(n)} = \sum_{i_n} L^{(n)i_n}u_i^{(n)i_n}, \quad \theta_3^{[n-1]} \leq \theta_3 \leq \theta_3^{[n]}, \tag{21}$$

$$\varepsilon_{ij}^{(n)} = \sum_{i_n} L^{(n)i_n}\varepsilon_{ij}^{(n)i_n}, \quad \theta_3^{[n-1]} \leq \theta_3 \leq \theta_3^{[n]}, \tag{22}$$

where $u_i^{(n)i_n}(\theta_1, \theta_2)$ and $\varepsilon_{ij}^{(n)i_n}(\theta_1, \theta_2)$ are the displacements and strains of SaS given by

$$u_i^{(n)i_n} = u_i\left(\theta_3^{(n)i_n}\right), \tag{23}$$

$$\varepsilon_{ij}^{(n)i_n} = \varepsilon_{ij}\left(\theta_3^{(n)i_n}\right). \tag{24}$$

The use of Eqs. (20), (21), (23) and (24) leads to the following strain–displacement relationships:

$$2\varepsilon_{\alpha\beta}^{(n)i_n} = \frac{1}{c_\beta^{(n)i_n}}\lambda_{\alpha\beta}^{(n)i_n} + \frac{1}{c_\alpha^{(n)i_n}}\lambda_{\beta\alpha}^{(n)i_n},$$

$$2\varepsilon_{\alpha3}^{(n)i_n} = \frac{1}{c_\alpha^{(n)i_n}}\lambda_{3\alpha}^{(n)i_n} + \beta_\alpha^{(n)i_n}, \quad \varepsilon_{33}^{(n)i_n} = \beta_3^{(n)i_n}, \tag{25}$$

where $\lambda_{i\alpha}^{(n)i_n}(\theta_1,\theta_2)$ are the strain parameters of SaS; $\beta_i^{(n)i_n}(\theta_1,\theta_2)$ are the values of the derivative of displacements with respect to thickness coordinate θ_3 at SaS defined as

$$\lambda_{\alpha\alpha}^{(n)i_n} = \lambda_{\alpha\alpha}\left(\theta_3^{(n)i_n}\right) = \frac{1}{A_\alpha}u_{\alpha,\alpha}^{(n)i_n} + B_\alpha u_\beta^{(n)i_n} + k_\alpha u_3^{(n)i_n} \quad \text{for} \quad \beta \neq \alpha,$$

$$\lambda_{\beta\alpha}^{(n)i_n} = \lambda_{\beta\alpha}\left(\theta_3^{(n)i_n}\right) = \frac{1}{A_\alpha}u_{\beta,\alpha}^{(n)i_n} - B_\alpha u_\alpha^{(n)i_n} \quad \text{for} \quad \beta \neq \alpha,$$

$$\lambda_{3\alpha}^{(n)i_n} = \lambda_{3\alpha}\left(\theta_3^{(n)i_n}\right) = \frac{1}{A_\alpha}u_{3,\alpha}^{(n)i_n} - k_\alpha u_\alpha^{(n)i_n}, \tag{26}$$

$$\beta_i^{(n)i_n} = u_{i,3}\left(\theta_3^{(n)i_n}\right) = \sum_{j_n} M^{(n)j_n}\left(\theta_3^{(n)i_n}\right)u_i^{(n)j_n}. \tag{27}$$

As can be seen from Eq. (27), the key functions $\beta_i^{(n)i_n}$ of the thermoelastic laminated shell formulation are represented as a linear combination of displacements of SaS of the nth layer $u_i^{(n)j_n}$.

Remark 2 Strain–displacement relationships (25)–(27) exactly represent all rigid-body motions of the laminated shell in any surface curvilinear coordinates. The proof of this statement can be given by using the results [24].

4 Variational formulation of heat conduction problem

The variational equation for the thermal laminated FG shell is written as

$$\delta J = 0, \tag{28}$$

where J is the basic functional of the heat conduction theory given by

$$J = \frac{1}{2}\iint_\Omega \sum_n \int_{\theta_3^{[n-1]}}^{\theta_3^{[n]}} q_i^{(n)}\Gamma_i^{(n)} A_1A_2c_1c_2 d\theta_1 d\theta_2 d\theta_3 - \iint_{\bar{\Omega}} TQ_n d\Omega, \tag{29}$$

where $q_i^{(n)}$ are the components of the heat flux vector of the nth layer; Q_n is the specified heat flux on the boundary surface $\bar{\Omega} = \Omega^{[0]} + \Omega^{[N]} + \Sigma$, where Σ is the edge boundary surface of a shell.

Substituting Eq. (6) in Eq. (29) and introducing heat flux resultants

$$R_i^{(n)i_n} = \int_{\theta_3^{[n-1]}}^{\theta_3^{[n]}} q_i^{(n)} L^{(n)i_n} c_1c_2 d\theta_3, \tag{30}$$

one obtains

$$J = \frac{1}{2}\iint_\Omega \sum_n \sum_{i_n} R_i^{(n)i_n}\Gamma_i^{(n)i_n} A_1A_2 d\theta_1 d\theta_2 - \iint_{\bar{\Omega}} TQ_n d\Omega. \tag{31}$$

As constitutive equations, we accept the Fourier's heat conduction equations

$$q_i^{(n)} = -k_{ij}^{(n)}\Gamma_j^{(n)}, \quad \theta_3^{[n-1]} \le \theta_3 \le \theta_3^{[n]}, \tag{32}$$

where $k_{ij}^{(n)}$ are the thermal conductivities of the nth layer.

Next, we introduce the fifth assumption of the proposed laminated FG shell formulation. Let us assume that thermal conductivities of the nth layer are distributed through the thickness of the shell as follows:

$$k_{ij}^{(n)} = \sum_{i_n} L^{(n)i_n} k_{ij}^{(n)i_n}, \quad \theta_3^{[n-1]} \le \theta_3 \le \theta_3^{[n]} \tag{33}$$

that is extensively utilized in this paper, where $k_{ij}^{(n)i_n}$ are the values of thermal conductivities on SaS of the nth layer.

The use of Eqs. (6), (32) and (33) into Eq. (30) leads to

$$R_i^{(n)i_n} = -\sum_{j_n,k_n} \Lambda^{(n)i_nj_nk_n} k_{ij}^{(n)j_n}\Gamma_j^{(n)k_n}, \tag{34}$$

where

$$\Lambda^{(n)i_nj_nk_n} = \int_{\theta_3^{[n-1]}}^{\theta_3^{[n]}} L^{(n)i_n} L^{(n)j_n} L^{(n)k_n} c_1 c_2 d\theta_3. \tag{35}$$

5 Variational formulation of thermoelastic shell problem

The variational equation for the thermoelastic laminated FG shell in the case of conservative loading [19] can be written as

$$\delta \Pi = 0, \tag{36}$$

where

$$\Pi = \iint_{\Omega} \sum_n \int_{\theta_3^{[n-1]}}^{\theta_3^{[n]}} F^{(n)} A_1 A_2 c_1 c_2 d\theta_1 d\theta_2 d\theta_3 - W, \tag{37}$$

$$F^{(n)} = \frac{1}{2}\left(\sigma_{ij}^{(n)} \varepsilon_{ij}^{(n)} - \eta^{(n)} \Theta^{(n)}\right), \tag{38}$$

$$W = \iint_{\Omega} \left(c_1^{[N]} c_2^{[N]} p_i^+ u_i^{[N]} - c_1^{[0]} c_2^{[0]} p_i^- u_i^{[0]}\right) A_1 A_2 d\theta_1 d\theta_2 + W_{\Sigma}, \tag{39}$$

where $F^{(n)}$ is the free-energy density of the nth layer; $\sigma_{ij}^{(n)}$ are the components of the stress tensor of the nth layer; $\eta^{(n)}$ is the entropy density of the nth layer; $u_i^{[0]} = u_i^{(1)1}$ and $u_i^{[N]} = u_i^{(N)I_N}$ are the displacements of the bottom and top surfaces $\Omega^{[0]}$ and $\Omega^{[N]}$; $c_\alpha^{[0]} = 1 + k_\alpha \theta_3^{[0]}$ and $c_\alpha^{[N]} = 1 + k_\alpha \theta_3^{[N]}$ are the components of the shifter tensor at the bottom and top surfaces; p_i^- and p_i^+ are the loads acting on the bottom and top surfaces; W_Σ is the work done by external loads applied to the edge surface Σ; $\Theta^{(n)}$ is the temperature rise from the initial reference temperature T_0 defined as

$$\Theta^{(n)} = T^{(n)} - T_0. \tag{40}$$

Substituting the strain distribution (22) and temperature distribution

$$\Theta^{(n)} = \sum_{i_n} L^{(n)i_n} \Theta^{(n)i_n}, \quad \theta_3^{[n-1]} \le \theta_3 \le \theta_3^{[n]}, \tag{41}$$

which follows from Eqs. (5) and (40) into Eqs. (37) and (38), and introducing stress resultants

$$H_{ij}^{(n)i_n} = \int_{\theta_3^{[n-1]}}^{\theta_3^{[n]}} \sigma_{ij}^{(n)} L^{(n)i_n} c_1 c_2 d\theta_3 \tag{42}$$

and entropy resultants

$$S^{(n)i_n} = \int_{\theta_3^{[n-1]}}^{\theta_3^{[n]}} \eta^{(n)} L^{(n)i_n} c_1 c_2 d\theta_3, \tag{43}$$

one derives

$$\Pi = \frac{1}{2} \iint_{\Omega} \sum_n \sum_{i_n} \left(H_{ij}^{(n)i_n} \varepsilon_{ij}^{(n)i_n} - S^{(n)i_n} \Theta^{(n)i_n}\right) A_1 A_2 d\theta_1 d\theta_2 - W. \tag{44}$$

For simplicity, we consider the case of linear thermoelastic materials. Therefore, the constitutive equations [38] are expressed as follows:

$$\sigma_{ij}^{(n)} = C_{ijk\ell}^{(n)} \varepsilon_{k\ell}^{(n)} - \gamma_{ij}^{(n)} \Theta^{(n)}, \quad \theta_3^{[n-1]} \le \theta_3 \le \theta_3^{[n]}, \tag{45}$$

$$\eta^{(n)} = \gamma_{ij}^{(n)} \varepsilon_{ij}^{(n)} + \chi^{(n)} \Theta^{(n)}, \quad \theta_3^{[n-1]} \le \theta_3 \le \theta_3^{[n]}, \tag{46}$$

where $C_{ijkl}^{(n)}$ are the elastic constants of the nth layer; $\gamma_{ij}^{(n)}$ are the thermal stress coefficients of the nth layer; $\chi^{(n)}$ is the entropy-temperature coefficient given by

$$\chi^{(n)} = \rho^{(n)} c_v^{(n)} / T_0, \tag{47}$$

where $\rho^{(n)}$ and $c_v^{(n)}$ are the mass density and the specific heat per unit mass of the nth layer at constant strain.

Finally, we introduce the sixth assumption of the thermoelastic FG shell formulation. Assume that material constants are distributed through the thickness of the nth layer as accepted throughout the paper

$$C_{ijkl}^{(n)} = \sum_{i_n} L^{(n)i_n} C_{ijkl}^{(n)i_n}, \quad \theta_3^{[n-1]} \le \theta_3 \le \theta_3^{[n]}, \tag{48}$$

$$\gamma_{ij}^{(n)} = \sum_{i_n} L^{(n)i_n} \gamma_{ij}^{(n)i_n}, \quad \theta_3^{[n-1]} \le \theta_3 \le \theta_3^{[n]}, \tag{49}$$

$$\chi^{(n)} = \sum_{i_n} L^{(n)i_n} \chi^{(n)i_n}, \quad \theta_3^{[n-1]} \le \theta_3 \le \theta_3^{[n]}, \tag{50}$$

where $C_{ijkl}^{(n)i_n}$, $\gamma_{ij}^{(n)i_n}$ and $\chi^{(n)i_n}$ are the values of material constants on SaS of the nth layer.

Substituting constitutive Eqs. (45) and (46) respectively in Eqs. (42) and (43), and taking into account the through-thickness distributions (22), (41), (48), (49) and (50), we arrive at the final expressions for stress and entropy resultants

$$H_{ij}^{(n)i_n} = \sum_{j_n, k_n} \Lambda^{(n)i_n j_n k_n} \left(C_{ijk\ell}^{(n)j_n} \varepsilon_{k\ell}^{(n)k_n} - \gamma_{ij}^{(n)j_n} \Theta^{(n)k_n} \right), \tag{51}$$

$$S^{(n)i_n} = \sum_{j_n, k_n} \Lambda^{(n)i_n j_n k_n} \left(\gamma_{ij}^{(n)j_n} \varepsilon_{k\ell}^{(n)k_n} + \chi^{(n)j_n} \Theta^{(n)k_n} \right), \tag{52}$$

where $\Lambda^{(n)i_n j_n k_n}$ are the definite integrals defined by Eq. (35).

6 Analytical solution for laminated FG cylindrical panels in cylindrical bending

In this section, we study a laminated anisotropic FG cylindrical panel in cylindrical bending subjected to thermomechanical loading. The boundary conditions for the simply supported shell with edges maintained at the reference temperature are written as

$$\sigma_{11}^{(n)} = \sigma_{12}^{(n)} = u_3^{(n)} = \Theta^{(n)} = 0 \quad \text{at} \quad \theta_1 = 0 \quad \text{and} \quad \theta_1 = L, \tag{53}$$

where θ_1 is the circumferential coordinate; $L = \varphi R$ is the length of the middle circular arc; R is the radius; φ is the arc angle. To satisfy the boundary conditions, we search for the analytical solution by a method of the Fourier series expansion

$$\Theta^{(n)i_n} = \sum_r \Theta_r^{(n)i_n} \sin \frac{r\pi\theta_1}{L}, \tag{54}$$

$$u_1^{(n)i_n} = \sum_r u_{1r}^{(n)i_n} \cos \frac{r\pi\theta_1}{L}, \quad u_2^{(n)i_n} = \sum_r u_{2r}^{(n)i_n} \cos \frac{r\pi\theta_1}{L},$$

$$u_3^{(n)i_n} = \sum_r u_{3r}^{(n)i_n} \sin \frac{r\pi\theta_1}{L}, \tag{55}$$

where r is the wave number. The external loads are also expanded in Fourier series.

The use of Fourier series (54) and (55) in Eqs. (10), (11), (25), (26), (27), (31), (34), (39), (40), (44), (51) and (52) yields

$$J = \sum_r J_r \left(\Theta_r^{(n)i_n} \right), \tag{56}$$

$$\Pi = \sum_r \Pi_r \left(u_{ir}^{(n)i_n}, \Theta_r^{(n)i_n} \right). \tag{57}$$

Invoking variational Eqs. (28), (56) and (36), (57), we arrive at the following systems of linear algebraic equations:

$$\frac{\partial J_r}{\partial \Theta_r^{(n)i_n}} = 0, \tag{58}$$

$$\frac{\partial \Pi_r}{\partial u_{ir}^{(n)i_n}} = 0 \tag{59}$$

of orders K and 3 K, where $K = \sum_n I_n - N + 1$ is the total number of SaS. First, we solve the linear system of algebraic Eqs. (58) using the method of Gaussian elimination. Then the linear system (59) is solved by the same method.

The described algorithm was performed with the Symbolic Math Toolbox, which incorporates symbolic computations into the numeric environment of MATLAB. This permits the derivation of analytical solutions for laminated anisotropic cylindrical panels in cylindrical bending in the framework of the SaS formulation, which asymptotically approach the 3D exact solutions of thermoelasticity as $I_n \to \infty$.

6.1 Single-layer metal/ceramic composite cylindrical panel

Consider a FG composite cylindrical panel fabricated by mixing metal and ceramic phases. The simply supported shell is subjected on the top surface by the sinusoidally distributed temperature whereas the bottom surface is maintained at the reference temperature 293 K, that is,

$$\Theta^+ = \Theta_0 \sin \frac{\pi\theta_1}{L}, \quad \Theta^- = 0, \tag{60}$$

where $\Theta_0 = 1\,\text{K}$. The geometric parameters of the shell are chosen to be $R = 1\,\text{m}$, $\varphi = \pi/2$ and $L = \pi/2\,\text{m}$. It is supposed that the metal phase is the aluminum with material properties $E_{\text{m}} = 7 \times 10^{10}\,\text{Pa}$,

$\nu_m = 0.3$, $\alpha_m = 23.4 \times 10^{-6}\,1/\mathrm{K}$, $k_m = 233\,\mathrm{W/mK}$, $\rho_m = 2707\,\mathrm{Kg/m^3}$ and $c_m = 896\,\mathrm{J/KgK}$, whereas material properties of the thermal ceramic (SiC) barrier are $E_c = 4.27 \times 10^{11}$ Pa, $\nu_c = 0.17$, $\alpha_c = 4.3 \times 10^{-6}$ 1/K, $k_c = 65$ W/mK, $\rho_c = 3100\,\mathrm{Kg/m^3}$ and $c_c = 670\,\mathrm{J/Kg\,K}$. The material properties of metal and ceramic phases are presented in papers [47, 48].

For evaluating the effective material properties through the thickness of the FG shell, the self-consistent method is utilized. The shear modulus [15] is given implicitly by

$$\left(\frac{V_m K_m}{K_m + 4G/3} + \frac{V_c K_c}{K_c + 4G/3}\right) + 5\left(\frac{V_m G_c}{G - G_c} + \frac{V_c G_m}{G - G_m}\right) + 2 = 0, \tag{61}$$

where K_m, K_c and G_m, G_c are the bulk and shear moduli of metal and ceramic phases; V_m and V_c are the volume fractions of metal and ceramic phases defined as

$$K_m = \frac{E_m}{3(1 - 2\nu_m)}, \quad K_c = \frac{E_c}{3(1 - 2\nu_c)}, \tag{62}$$

$$G_m = \frac{E_m}{2(1 + \nu_m)}, \quad G_c = \frac{E_c}{2(1 + \nu_c)}, \tag{63}$$

$$V_m = 1 - V_c, \quad V_c = V_c^- + \left(V_c^+ - V_c^-\right)(0.5 + z)^\gamma, \quad z = \theta_3/h, \tag{64}$$

where V_c^- and V_c^+ are the volume fractions of the ceramic on the bottom and top surfaces; γ is the material gradient index. Solving the quartic Eq. (61), which has precisely one positive root, we can find G and then the bulk modulus from the following formula [15]:

$$K = \left[\frac{V_m}{K_m + 4G/3} + \frac{V_c}{K_c + 4G/3}\right]^{-1} - 4G/3. \tag{65}$$

The thermal conductivity [13] is also given implicitly by

$$\frac{V_m(k_m - k)}{k_m + 2k} + \frac{V_c(k_c - k)}{k_c + 2k} = 0. \tag{66}$$

The thermal expansion coefficient [30, 40] is defined as

$$\alpha = \alpha_m + \frac{(\alpha_c - \alpha_m)(1/K - 1/K_m)}{1/K_c - 1/K_m}. \tag{67}$$

The product $c\rho$ can be easily found using the rule of mixture [48]

$$c\rho = c_m \rho_m V_m + c_c \rho_c V_c. \tag{68}$$

To compare the results derived with the exact solution of thermoelasticity [36], we accept $V_c^- = 0.2$, $V_c^+ = 0.8$ and $\gamma = 2$, and introduce dimensionless variables at crucial points as follows:

$$\bar{u}_1 = 10^3 h u_1(0, z)/L^2 \alpha_m \Theta_0, \quad \bar{u}_3 = 10^3 h u_3(L/2, z)/L^2 \alpha_m \Theta_0,$$

$$\bar{\sigma}_{ii} = 10^3 h \sigma_{ii}(L/2, z)/L E_m \alpha_m \Theta_0, \quad \bar{\sigma}_{13} = 10^3 h \sigma_{13}(0, z)/L E_m \alpha_m \Theta_0,$$

$$\bar{\Theta} = \Theta(L/2, z)/\Theta_0, \quad \bar{q}_3 = -h q_3(L/2, z)/k_m \Theta_0,$$

$$\bar{\eta} = \eta(L/2, z)/E_m \alpha_m^2 \Theta_0, \quad z = \theta_3/h.$$

Tables 1 and 2 show the results of the convergence study due to increasing the number of SaS inside the shell body. A comparison with the exact solution [36] for $L/h = 10$ is presented. It is seen that the SaS formulation gives the possibility to find basic shell variables with a specified accuracy (five right digits) by using the sufficiently large number of SaS. Figure 2 displays distributions of the temperature, heat flux, transverse displacement and stresses through the thickness of the cylindrical panel for different values of the ratio L/h employing 15 SaS. These results demonstrate convincingly the high potential of the developed SaS formulation because the boundary conditions on the bottom and top surfaces of the cylindrical panel for transverse stresses are satisfied exactly.

6.2 Angle-ply cylindrical panel covered with metal/ceramic layer

Here, we study a two-layer cylindrical panel [45/−45] composed of the graphite/epoxy composite and covered with the metal/ceramic barrier on its top surface. Thus, a three-layer shell with the stacking sequence [45/−45/FGM] and ply thicknesses [0.25 h/0.25 h/0.5 h] is considered. The mechanical properties of the graphite/epoxy composite are taken as follows: $E_L = E_0$, $E_T = E_0/10$, $G_{LT} = E_0/20$, $G_{TT} = E_0/50$,

Table 1 Results for a single-layer metal/ceramic cylindrical panel in cylindrical bending for $L/h = 2$

I_1	$\bar{u}_1(0)$	$\bar{u}_3(0)$	$\bar{\sigma}_{11}(0)$	$\bar{\sigma}_{22}(0)$	$\bar{\sigma}_{13}(0)$	$\bar{\sigma}_{13}(0.25)$	$\bar{\sigma}_{33}(0)$	$\bar{\Theta}(0)$	$\bar{q}_3(-0.5)$	$\bar{\eta}(0)$
3	−28.286	16.389	−87.970	−258.06	−5.1509	15.604	−79.022	0.37950	0.42233	78.962
5	−32.789	9.2840	−60.883	−232.58	−0.54364	24.018	−8.4753	0.37908	0.64087	79.025
7	−32.793	9.5783	−60.652	−232.04	0.66682	19.708	−8.5118	0.37999	0.64503	79.215
9	−32.781	9.5611	−60.664	−232.96	0.83004	19.086	−8.0702	0.38004	0.64824	79.226
11	−32.780	9.5611	−60.686	−232.98	0.87520	19.139	−8.1265	0.38003	0.64863	79.225
13	−32.780	9.5612	−60.687	−232.98	0.86928	19.124	−8.1280	0.38003	0.64873	79.225
15	−32.780	9.5612	−60.687	−232.98	0.86979	19.126	−8.1283	0.38003	0.64876	79.225
17	−32.780	9.5612	−60.687	−232.98	0.86980	19.126	−8.1282	0.38003	0.64877	79.225

Table 2 Results for a single-layer metal/ceramic cylindrical panel in cylindrical bending for $L/h = 10$

I_1	$\bar{u}_1(0)$	$\bar{u}_3(0)$	$\bar{\sigma}_{11}(0)$	$\bar{\sigma}_{22}(0)$	$\bar{\sigma}_{13}(0)$	$\bar{\sigma}_{13}(0.25)$	$\bar{\sigma}_{33}(0)$	$\bar{\Theta}(0)$	$\bar{q}_3(-0.5)$	$\bar{\eta}(0)$
3	8.1080	32.978	−19.939	−58.384	−0.47111	0.78287	−19.737	0.42497	0.57060	88.406
5	7.3645	31.439	−12.309	−50.632	−0.17924	1.0392	−1.0593	0.41657	0.65946	86.856
7	7.4339	31.593	−11.928	−50.288	−0.15207	0.78309	−0.016783	0.41678	0.66600	86.910
9	7.4320	31.589	−11.916	−50.276	−0.14938	0.76662	0.019898	0.41679	0.66610	86.912
11	7.4321	31.589	−11.917	−50.277	−0.14928	0.76741	0.016781	0.41679	0.66608	86.912
13	7.4321	31.589	−11.918	−50.277	−0.14933	0.76720	0.016023	0.41679	0.66608	86.912
15	7.4321	31.589	−11.918	−50.277	−0.14933	0.76719	0.015958	0.41679	0.66608	86.912
17	7.4321	31.589	−11.918	−50.277	−0.14933	0.76720	0.015962	0.41679	0.66608	86.912
Exact	7.4320	31.589	−11.917	−50.277	−0.14933	0.76719	0.015962	0.41678	0.66608	

$\nu_{LT} = \nu_{TT} = 0.25$, $\alpha_L = \alpha_0$, $\alpha_T = 7.2\alpha_0$, $k_L = 100k_0$, $k_T = k_0$, $\rho = 1800\,\mathrm{Kg/m^3}$ and $c_v = 900\,\mathrm{J/KgK}$, where $E_0 = 2\times10^{11}\,\mathrm{Pa}$, $\alpha_0 = 5\times10^{-6}\,1/\mathrm{K}$ and $k_0 = 0.5\,\mathrm{W/mK}$. The mechanical properties of the metal/ceramic composite are given in Sect. 6.1.

To evaluate the effective material properties through the thickness of the metal/ceramic barrier, the Mori–Tanaka scheme [4, 14, 31] is invoked

$$K = K_m + \frac{V_c(K_c - K_m)}{1 + V_m(K_c - K_m)/(K_m + 4G_m/3)}, \tag{69}$$

$$G = G_m + \frac{V_c(G_c - G_m)}{1 + V_m(G_c - G_m)/(G_m + f_m)}, \quad f_m = \frac{G_m(9K_m + 8G_m)}{6(K_m + 2G_m)}, \tag{70}$$

$$k = k_m + \frac{V_c(k_c - k_m)}{1 + V_m(k_c - k_m)/(3k_m)} \tag{71}$$

with a specific distribution of the volume fraction of the ceramic phase

$$V_c = V_c^- + \left(V_c^+ - V_c^-\right)(2z)^\gamma, \quad 0 \le z \le 0.5, \quad z = \theta_3/h, \tag{72}$$

where $V_c^- = 0$, $V_c^+ = 0.5$ and $\gamma = 2$. The thermal expansion coefficient α and the product $c\rho$ can be found by Eqs. (67) and (68).The panel is loaded on the top surface by the sinusoidally distributed temperature according to Eq. (60) with $\Theta_0 = 1\,\mathrm{K}$ and $T_0 = 293\,\mathrm{K}$. The geometric parameters of the shell are taken to be $R = 1\,\mathrm{m}$, $\varphi = \pi/2$ and $L = \pi/2\,\mathrm{m}$. To analyze the derived results efficiently, we introduce the following dimensionless variables at crucial points:

$$\bar{u}_1 = 10hu_1(0,z)/R^2\alpha_m\Theta_0, \quad \bar{u}_2 = 10u_2(0,z)/R\alpha_m\Theta_0, \quad \bar{u}_3 = 10hu_3(L/2,z)/R^2\alpha_m\Theta_0,$$

$$\bar{\sigma}_{11} = 10\sigma_{11}(L/2,z)/E_m\alpha_m\Theta_0, \quad \bar{\sigma}_{12} = 10\sigma_{12}(L/2,z)/E_m\alpha_m\Theta_0,$$

$$\bar{\sigma}_{\alpha3} = 10^2R\sigma_{\alpha3}(0,z)/hE_m\alpha_m\Theta_0, \quad \bar{\sigma}_{33} = 10^2R\sigma_{33}(L/2,z)/hE_m\alpha_m\Theta_0,$$

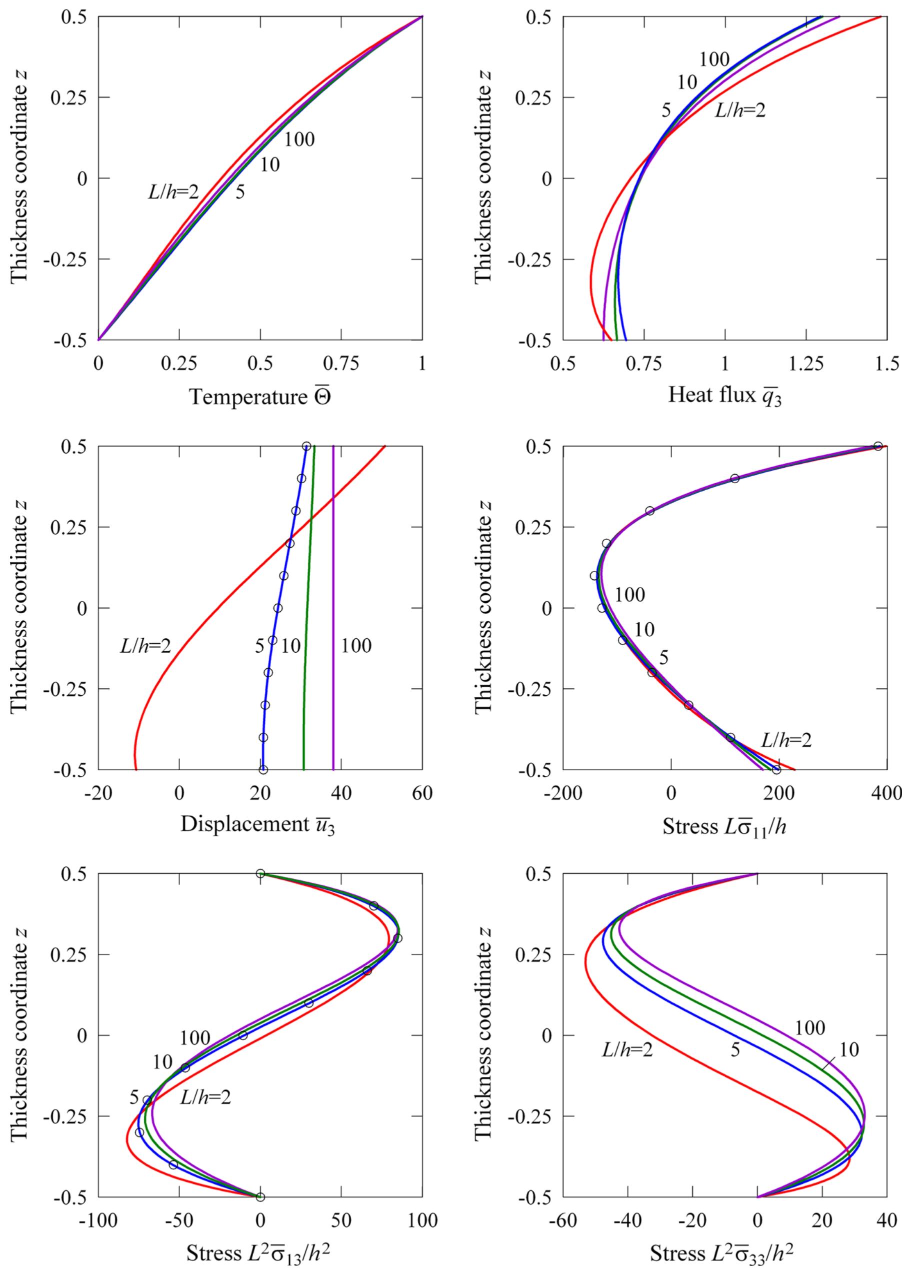

Fig. 2 Through-thickness distributions of the temperature, heat flux, transverse displacement and stresses for a metal/ceramic cylindrical panel: SaS solution (*solid line*) with $I_1 = 15$ and exact solution (*circle*) [36]

$$\bar{\Theta} = \Theta(L/2, z)/\Theta_0, \quad \bar{q}_3 = -10Rq_3(L/2, z)/k_{\mathrm{m}}\Theta_0,$$

$$\bar{\eta} = \eta(L/2, z)/E_{\mathrm{m}}\alpha_{\mathrm{m}}^2\Theta_0, \quad z = \theta_3/h.$$

The data listed in Tables 3 and 4 show that the SaS method permits the derivation of analytical solutions for thick angle-ply FG cylindrical panels with a prescribed accuracy using the sufficient number of SaS. Note that the transverse components of the heat flux vector and the stress tensor are calculated at the interface between the shell and the metal/ceramic barrier and, therefore, their both values are presented. As turned out, the SaS method provides five right digits for these functions at the interface taking 14 SaS inside the layer, i.e. 40 SaS inside the moderately thick shell. Figures 3 and 4 display through-thickness distributions of the temperature, displacements, heat flux and stresses for different slenderness ratios R/h by

Table 3 Results for a three-layer cylindrical panel [45/−45/FGM] in cylindrical bending for $R/h = 2$

I_n	$\bar{u}_1(0.5)$	$\bar{u}_3(0.5)$	$\bar{\sigma}_{11}(0.5)$	$\bar{\sigma}_{12}(0.5)$	$\bar{\sigma}_{13}(0)$	$\bar{\sigma}_{23}(0)$	$\bar{\sigma}_{33}(0)$	$\bar{\Theta}(-0.125)$	$\bar{q}_3(0)$	$\bar{\eta}(-0.125)$
3	−1.9222	2.6979	8.9220	0.49532	−10.533	3.0697	−9.1718	0.35077	0.23852	51.348
					−2.1994	3.3288	37.686		0.076062	
5	−1.9078	2.8350	9.2064	0.50292	−9.8213	3.4321	2.6222	0.35297	0.26868	51.605
					−10.668	3.4514	3.2087		0.21965	
7	−1.9083	2.8273	9.2168	0.50240	−9.7972	3.4434	2.7407	0.35334	0.27040	51.658
					−9.7341	3.4420	2.7462		0.27258	
9	−1.9083	2.8273	9.2176	0.50240	−9.7986	3.4416	2.7475	0.35337	0.27027	51.663
					−9.7877	3.4416	2.7425		0.27258	
11	−1.9083	2.8273	9.2176	0.50240	−9.7990	3.4415	2.7482	0.35336	0.27025	51.663
					−9.7954	3.4415	2.7466		0.27035	
13	−1.9083	2.8273	9.2176	0.50240	−9.7991	3.4414	2.7483	0.35336	0.27025	51.663
					−9.7978	3.4414	2.7477		0.27029	
15	−1.9083	2.8273	9.2176	0.50240	−9.7991	3.4414	2.7484	0.35336	0.27025	51.663
					−9.7986	3.4414	2.7481		0.27027	
17	−1.9083	2.8273	9.2176	0.50240	−9.7991	3.4414	2.7484	0.35336	0.27025	51.663
					−9.7989	3.4414	2.7482		0.27026	

Table 4 Results for a three-layer cylindrical panel [45/−45/FGM] in cylindrical bending for $R/h = 10$

I_n	$\bar{u}_1(0.5)$	$\bar{u}_3(0.5)$	$\bar{\sigma}_{11}(0.5)$	$\bar{\sigma}_{12}(0.5)$	$\bar{\sigma}_{13}(0)$	$\bar{\sigma}_{23}(0)$	$\bar{\sigma}_{33}(0)$	$\bar{\Theta}(-0.125)$	$\bar{q}_3(0)$	$\bar{\eta}(-0.125)$
3	0.82088	2.8152	10.685	0.30850	−11.586	1.4213	1.4269	0.72113	0.48153	105.24
					−3.6706	1.9928	253.33		0.31189	
5	0.86170	2.9161	10.850	0.32499	−11.359	1.9974	5.1356	0.72110	0.48578	105.23
					−11.962	2.0054	6.2001		0.47310	
7	0.85926	2.9100	10.855	0.32399	−11.373	1.9955	5.1404	0.72110	0.48582	105.23
					−11.349	1.9952	5.2629		0.48540	
9	0.85927	2.9101	10.857	0.32400	−11.373	1.9951	5.1407	0.72110	0.48582	105.23
					−11.370	1.9951	5.1486		0.48580	
11	0.85927	2.9101	10.857	0.32400	−11.373	1.9951	5.1407	0.72110	0.48582	105.23
					−11.372	1.9951	5.1406		0.48582	
13	0.85927	2.9101	10.857	0.32400	−11.373	1.9951	5.1407	0.72110	0.48582	105.23
					−11.373	1.9951	5.1406		0.48582	
15	0.85927	2.9101	10.857	0.32400	−11.373	1.9951	5.1407	0.72110	0.48582	105.23
					−11.373	1.9951	5.1407		0.48582	
17	0.85927	2.9101	10.857	0.32400	−11.373	1.9951	5.1407	0.72110	0.48582	105.23
					−11.373	1.9951	5.1407		0.48582	

choosing 13 SaS for each layer. As can be seen, the boundary conditions for transverse stresses on the bottom and top surfaces and the continuity conditions for a heat flux and transverse stresses at both interfaces are satisfied correctly.

7 Analytical solution for laminated FG cylindrical shells

In this section, we consider a laminated orthotropic cylindrical shell subjected to thermal and mechanical

Fig. 3 Through-thickness distributions of the temperature and displacements for a three-layer cylindrical panel [45/−45/FGM] with $I_1 = I_2 = I_3 = 13$

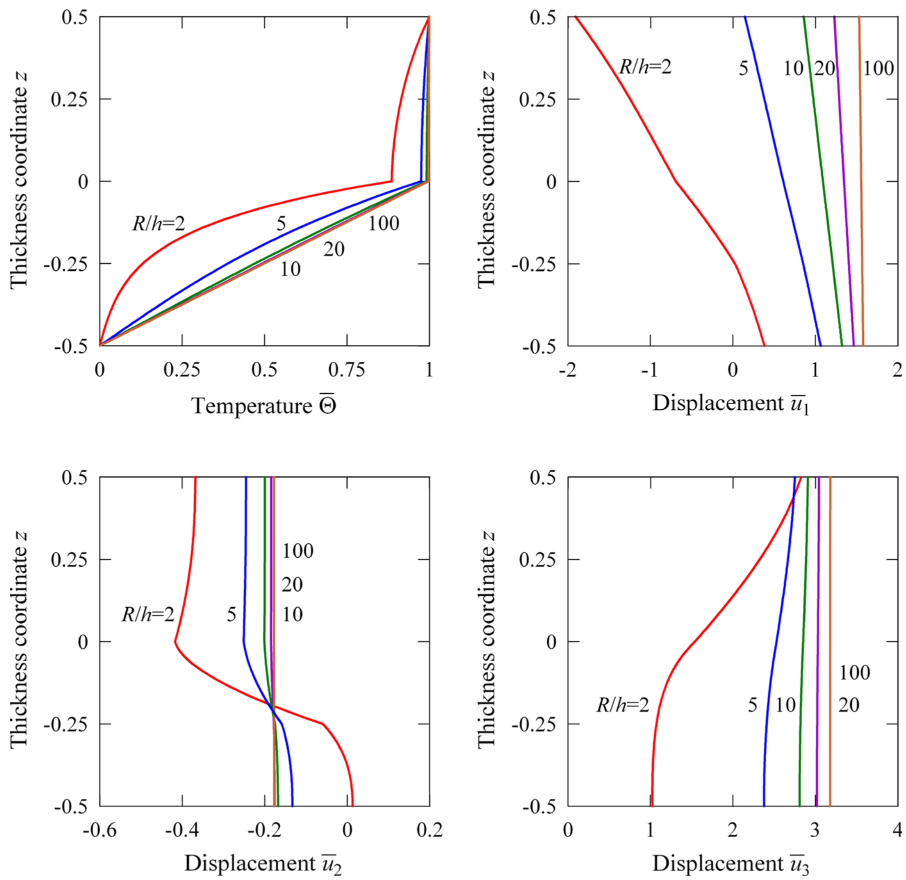

loading. Let the middle surface of the radius R be described by axial and circumferential coordinates θ_1 and θ_2. In this case, the boundary conditions for a simply supported cylindrical shell with the edges maintained at the reference temperature can be written as

$$\sigma_{11}^{(n)} = u_2^{(n)} = u_3^{(n)} = \Theta^{(n)} = 0 \quad \text{at} \quad \theta_1 = 0 \quad \text{and} \quad \theta_1 = a,$$

$$\sigma_{22}^{(n)} = u_1^{(n)} = u_3^{(n)} = \Theta^{(n)} = 0 \quad \text{at} \quad \theta_2 = 0 \quad \text{and} \quad \theta_2 = b, \tag{73}$$

where a is the length of the shell; $b = \varphi R$ is the length of the circular arc and φ is the arc angle. To satisfy the boundary conditions, we search for the analytical solution of the problem by a method of the double Fourier series expansion

$$\Theta^{(n)i_n} = \sum_{r,s} \Theta_{rs}^{(n)i_n} \sin\frac{r\pi\theta_1}{a} \sin\frac{s\pi\theta_2}{b}, \tag{74}$$

$$u_1^{(n)i_n} = \sum_{r,s} u_{1rs}^{(n)i_n} \cos\frac{r\pi\theta_1}{a} \sin\frac{s\pi\theta_2}{b},$$
$$u_2^{(n)i_n} = \sum_{r,s} u_{2rs}^{(n)i_n} \sin\frac{r\pi\theta_1}{a} \cos\frac{s\pi\theta_2}{b},$$
$$u_3^{(n)i_n} = \sum_{r,s} u_{3rs}^{(n)i_n} \sin\frac{r\pi\theta_1}{a} \sin\frac{s\pi\theta_2}{b}, \tag{75}$$

where r and s are the wave numbers in θ_1- and θ_2-directions. The external mechanical loads are also expanded in double Fourier series.

Substituting Fourier series (74) and (75) in Eqs. (10), (11), (25), (26), (27), (31), (34), (39) (40), (44), (51) and (52), one obtains

$$J = \sum_{r,s} J_{rs}\left(\Theta_{rs}^{(n)i_n}\right), \tag{76}$$

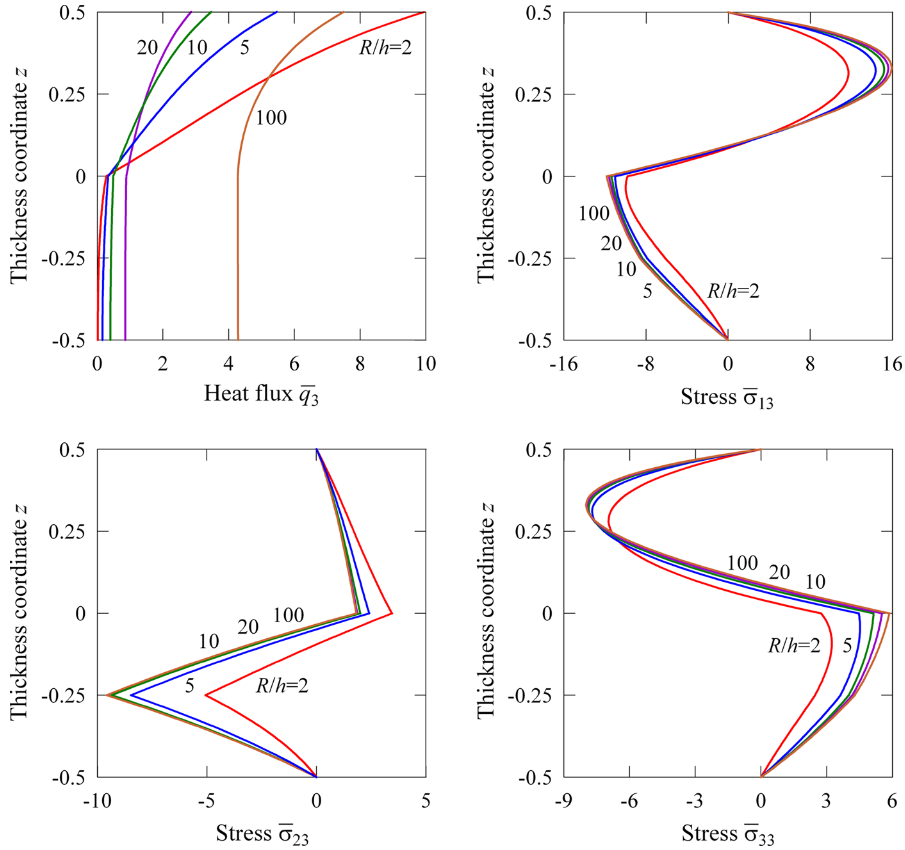

Fig. 4 Through-thickness distributions of the heat flux and stresses for a three-layer cylindrical panel [45/−45/FGM] with $I_1 = I_2 = I_3 = 13$

$$\Pi = \sum_{r,s} \Pi_{rs}\left(u_{irs}^{(n)i_n}, \Theta_{rs}^{(n)i_n}\right). \tag{77}$$

Using variational Eqs. (28), (76) and (36), (77), we arrive at two systems of linear algebraic equations

$$\frac{\partial J_{rs}}{\partial \Theta_{rs}^{(n)i_n}} = 0, \tag{78}$$

$$\frac{\partial \Pi_{rs}}{\partial u_{irs}^{(n)i_n}} = 0 \tag{79}$$

of orders K and $3K$, where K is the total number of SaS defined in Sect. 6. The linear systems (78) and (79) are solved independently by the Gaussian elimination method.

Table 5 Results for a single-layer metal/ceramic cylindrical shell for $R/h = 2$

I_1	$\bar{u}_1(0.5)$	$\bar{u}_2(0.5)$	$\bar{u}_3(0.5)$	$\bar{\sigma}_{11}(0.5)$	$\bar{\sigma}_{22}(0.5)$	$\bar{\sigma}_{12}(0.5)$	$\bar{\sigma}_{13}(0)$	$\bar{\sigma}_{23}(0)$	$\bar{\sigma}_{33}(0)$	$\bar{\Theta}(0)$	$\bar{q}_3(-0.5)$	$\bar{\eta}(0)$
3	−2.5424	−1.5393	30.845	−5.3359	3.8713	−4.4975	0.56580	5.9348	−25.316	0.43434	0.73737	94.251
5	−2.5397	−1.5852	30.872	−6.1923	3.1512	−4.5245	1.5326	11.283	−4.0027	0.43435	0.90909	94.431
7	−2.5355	−1.5843	30.806	−6.1897	3.1388	−4.5183	1.3799	11.256	−4.0410	0.43461	0.91050	94.484
9	−2.5355	−1.5844	30.806	−6.1890	3.1395	−4.5183	1.3638	11.259	−4.0376	0.43463	0.91186	94.490
11	−2.5355	−1.5843	30.806	−6.1891	3.1395	−4.5183	1.3676	11.263	−4.0390	0.43463	0.91199	94.490
13	−2.5355	−1.5843	30.806	−6.1892	3.1394	−4.5183	1.3667	11.262	−4.0389	0.43463	0.91202	94.490
15	−2.5355	−1.5843	30.806	−6.1892	3.1393	−4.5183	1.3670	11.263	−4.0387	0.43463	0.91203	94.490
17	−2.5355	−1.5843	30.806	−6.1892	3.1393	−4.5183	1.3669	11.263	−4.0387	0.43463	0.91203	94.490

The described algorithm was performed with the Symbolic Math Toolbox of MATLAB. This technique gives the possibility to derive the analytical solutions for laminated FG cylindrical shells with a specified accuracy, which asymptotically approach the 3D exact solutions of thermoelasticity as $I_n \to \infty$.

7.1 Two-phase composite cylindrical shell under temperature loading

Consider a single-layer FG cylindrical shell fabricated by mixing metal and ceramic phases. The shell is subjected on the top surface to sinusoidally distributed

Table 6 Results for a single-layer metal/ceramic cylindrical shell for $R/h = 10$

I_1	$\bar{u}_1(0.5)$	$\bar{u}_2(0.5)$	$\bar{u}_3(0.5)$	$\bar{\sigma}_{11}(0.5)$	$\bar{\sigma}_{22}(0.5)$	$\bar{\sigma}_{12}(0.5)$	$\bar{\sigma}_{13}(0)$	$\bar{\sigma}_{23}(0)$	$\bar{\sigma}_{33}(0)$	$\bar{\Theta}(0)$	$\bar{q}_3(-0.5)$	$\bar{\eta}(0)$
3	−5.1888	8.7907	24.985	−0.54135	4.5306	−2.5392	1.1008	2.3140	−133.41	0.44789	0.79156	97.474
5	−5.1689	8.6992	24.828	−1.7182	3.4238	−2.5682	3.1211	7.2866	−3.5090	0.44497	0.87090	97.050
7	−5.1658	8.6957	24.815	−1.6988	3.4379	−2.5656	3.1471	7.3990	−2.3474	0.44492	0.87511	97.042
9	−5.1658	8.6956	24.815	−1.6987	3.4380	−2.5656	3.1452	7.3997	−2.2913	0.44492	0.87532	97.043
11	−5.1658	8.6956	24.815	−1.6987	3.4380	−2.5656	3.1455	7.4002	−2.2919	0.44492	0.87533	97.043
13	−5.1658	8.6956	24.815	−1.6987	3.4380	−2.5656	3.1454	7.4001	−2.2918	0.44492	0.87533	97.043
15	−5.1658	8.6956	24.815	−1.6987	3.4380	−2.5656	3.1455	7.4001	−2.2918	0.44492	0.87533	97.043

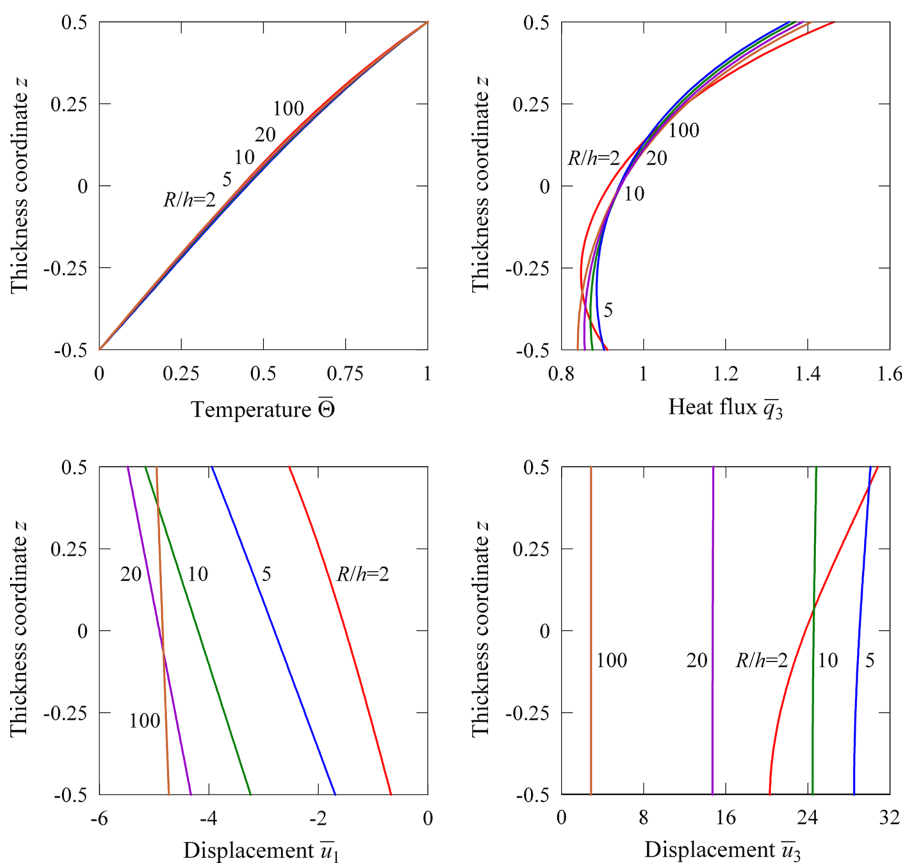

Fig. 5 Through-thickness distributions of the temperature, heat flux and displacements for a metal/ceramic cylindrical shell with $I_1 = 15$

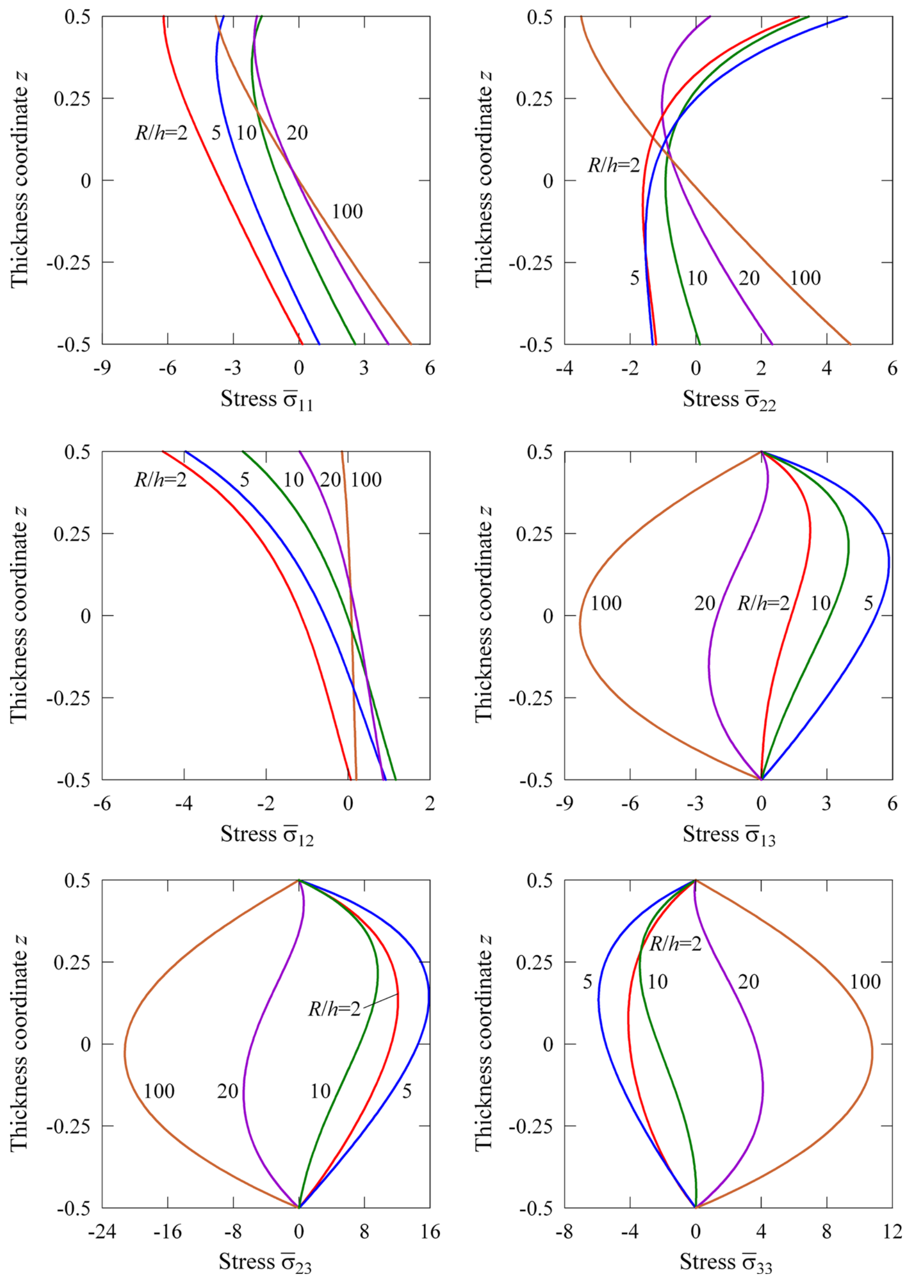

Fig. 6 Through-thickness distributions of stresses for a metal/ceramic cylindrical shell with $I_1 = 15$

temperature loading, whereas the bottom surface is maintained at the reference temperature 293 K, that is,

$$\Theta^+ = \Theta_0 \sin\frac{\pi\theta_1}{a}\sin\frac{\pi\theta_2}{b}, \quad \Theta^- = 0, \tag{80}$$

where $\Theta_0 = 1\,\mathrm{K}$. The geometric parameters of the shell are $a = 4\,\mathrm{m}$, $b = \pi/2\,\mathrm{m}$, $R = 1\,\mathrm{m}$ and $\varphi = \pi/2$. The material properties of metal and ceramic phases are presented in Sect. 6.1. For evaluating the effective material properties through the thickness of the FG shell, the Mori–Tanaka method with the use of Eqs. (62)–(64) and (67)–(71) is utilized.

For numerical calculations, we accept $V_c^- = 0$, $V_c^+ = 0.5$ and $\gamma = 2$ into Eq. (64) and introduce dimensionless variables

$$\bar{u}_1 = 10u_1(0, b/2, z)/R\alpha_\mathrm{m}\Theta_0,$$
$$\bar{u}_2 = 10u_2(a/2, 0, z)/R\alpha_\mathrm{m}\Theta_0,$$

$$\bar{u}_3 = 100hu_3(a/2,b/2,z)/R^2\alpha_\mathrm{m}\Theta_0,$$

$$\bar{\sigma}_{\alpha\alpha} = 10\sigma_{\alpha\alpha}(a/2,b/2,z)/E_\mathrm{m}\alpha_\mathrm{m}\Theta_0,\quad \bar{\sigma}_{12} = 10\sigma_{12}(0,0,z)/E_\mathrm{m}\alpha_\mathrm{m}\Theta_0,$$

$$\bar{\sigma}_{13} = 100R\sigma_{13}(0,b/2,z)/hE_\mathrm{m}\alpha_\mathrm{m}\Theta_0,\quad \bar{\sigma}_{23} = 100R\sigma_{23}(a/2,0,z)/hE_\mathrm{m}\alpha_\mathrm{m}\Theta_0,$$

$$\bar{\sigma}_{33} = 100R\sigma_{33}(a/2,b/2,z)/hE_\mathrm{m}\alpha_\mathrm{m}\Theta_0,$$

$$\bar{\Theta} = \Theta(a/2,b/2,z)/\Theta_0,\quad \bar{q}_3 = -hq_3(a/2,b/2,z)/k_\mathrm{m}\Theta_0,$$

$$\bar{\eta} = \eta(a/2,b/2,z)/E_\mathrm{m}\alpha_\mathrm{m}^2\Theta_0,\quad z = \theta_3/h.$$

The results of the convergence study are presented in Tables 5 and 6. It is seen that the SaS formulation provides five right digits (in fact, the better accuracy is possible) for all basic variables of thick FG cylindrical shells utilizing the sufficiently large number of SaS. Figures 5 and 6 show distributions of the temperature, heat flux, displacements and stresses through the thickness of the shell for different values of the slenderness ratio R/h by choosing 15 SaS inside the shell body. One can see that boundary conditions for the heat flux and transverse stresses on the bottom and top surfaces are satisfied again exactly.

8 Conclusions

The SaS formulation for the 3D analysis of steady-state problems for thermoelastic laminated FG shells has been developed. This formulation is based on choosing the SaS located at Chebyshev polynomial nodes throughout the layers. Such choice permits one to minimize uniformly the error due to Lagrange interpolation. The SaS formulation for laminated orthotropic and anisotropic shells is based on 3D constitutive equations and gives the possibility to obtain the analytical solutions for FG shells with a prescribed accuracy, which *asymptotically* approach the 3D exact solutions of thermoelasticity as the number of SaS goes to infinity.

Acknowledgments This work was supported by Russian Science Foundation (RSF) under Grant No 15-19-30002 and by Russian Ministry of Education and Science under Grant No 339.2014.

References

1. Alibeigloo A (2010) Exact solution for thermo-elastic response of functionally graded rectangular plates. Compos Struct 92:113–121
2. Alibeigloo A (2014) Three-dimensional thermo-elasticity solution of sandwich cylindrical panel with functionally graded core. Compos Struct 107:458–468
3. Alibeigloo A, Liew KM (2013) Thermoelastic analysis of functionally graded carbon nanotube-reinforced composite plate using theory of elasticity. Compos Struct 106:873–881
4. Benveniste Y (1987) A new approach to the application of Mori–Tanaka's theory in composite materials. Mech Mater 6:147–157
5. Birman V, Byrd LW (2007) Modeling and analysis of functionally graded materials and structures. Appl Mech Rev 60:195–216
6. Brischetto S, Carrera E (2011) Heat conduction and thermal analysis in multilayered plates and shells. Mech Res Commun 38:449–455
7. Brischetto S, Carrera E (2013) Static analysis of multilayered smart shells subjected to mechanical, thermal and electrical loads. Meccanica 48:1263–1287
8. Brogan WL (1985) Modern control theory. Prentice Hall, New Jersey
9. Burden RL, Faires JD (2010) Numerical analysis, 9th edn. Brooks/Cole, Cengage Learning, Boston
10. Carrera E (2003) Theories and finite elements for multilayered plates and shells: a unified compact formulation with numerical assessment and benchmarking. Arch Comput Meth Eng 10:215–296
11. Cheng ZQ, Batra RC (2000) Three-dimensional thermoelastic deformations of a functionally graded elliptic plate. Compos B 31:97–106
12. Gol'denveizer AN (1961) Theory of thin elastic shells. Pergamon Press, New York
13. Hashin Z (1968) Assessment of the self-consistent scheme approximation: conductivity of particulate composites. J Compos Mater 2:284–300
14. Hatta H, Taya M (1985) Effective thermal conductivity of a misoriented short fiber composite. J Appl Phys 58:2478–2486
15. Hill R (1965) A self-consistent mechanics of composite materials. J Mech Phys Solids 13:213–222
16. Jabbari M, Bahtui A, Eslami MR (2009) Axisymmetric mechanical and thermal stresses in thick short length FGM cylinders. Int J Pressure Vessels Piping 86:296–306
17. Jha DK, Kant T, Singh RK (2013) A critical review of recent research on functionally graded plates. Compos Struct 96:833–849
18. Kashtalyan M (2004) Three-dimensional elasticity solution for bending of functionally graded rectangular plates. Eur J Mech A/Solids 23:853–864
19. Kovalenko AD (1969) Thermoelasticity. Basic theory and applications. Wolters-Noordhoff, Groningen
20. Kulikov GM (2001) Refined global approximation theory of multilayered plates and shells. J Eng Mech 127:119–125
21. Kulikov GM, Carrera E (2008) Finite deformation higher-order shell models and rigid-body motions. Int J Solids Struct 45:3153–3172

22. Kulikov GM, Plotnikova SV (2011) Solution of statics problems for a three-dimensional elastic shell. Doklady Phys 56:448–451
23. Kulikov GM, Plotnikova SV (2012) On the use of sampling surfaces method for solution of 3D elasticity problems for thick shells. ZAMM J Appl Math Mech 92:910–920
24. Kulikov GM, Plotnikova SV (2013) Advanced formulation for laminated composite shells: 3D stress analysis and rigid-body motions. Compos Struct 95:236–246
25. Kulikov GM, Plotnikova SV (2014) Heat conduction analysis of laminated shells by a sampling surfaces method. Mech Res Commun 55:59–65
26. Kulikov GM, Plotnikova SV (2014) 3D exact thermoelastic analysis of laminated composite shells via sampling surfaces method. Compos Struct 115:120–130
27. Kulikov GM, Plotnikova SV (2015) Three-dimensional thermal stress analysis of laminated composite plates with general layups by a sampling surfaces method. Eur J Mech A/Solids 49:214–226
28. Kulikov GM, Plotnikova SV (2015) A sampling surfaces method and its implementation for 3D thermal stress analysis of functionally graded plates. Compos Struct 120:315–325
29. Kulikov GM, Plotnikova SV, Mamontov AA (2015) Coupled thermoelectroelastic stress analysis of piezoelectric shells. Compos Struct 124:65–76
30. Levin VM (1967) Thermal expansion coefficients of heterogeneous materials. Mekhanika Tverdogo Tela N2:88–94
31. Mori T, Tanaka K (1973) Average stress in matrix and average elastic energy of materials with misfitting inclusions. Acta Metall 21:571–574
32. Ootao Y (2011) Transient thermoelastic analysis for a multilayered thick strip with piecewise exponential nonhomogeneity. Compos B 42:973–981
33. Ootao Y, Ishihara M (2013) Three-dimensional solution for transient thermoelastic problem of a functionally graded rectangular plate with piecewise exponential law. Compos Struct 106:672–680
34. Ootao Y, Tanigawa Y (2007) Three-dimensional solution for transient thermal stresses of an orthotropic functionally graded rectangular plate. Compos Struct 80:10–20
35. Pagano NJ (1970) Exact solutions for rectangular bidirectional composites and sandwich plates. J Compos Mater 4:20–34
36. Pelletier JL, Vel SS (2006) An exact solution for the steady-state thermoelastic response of functionally graded orthotropic cylindrical shells. Int J Solids Struct 43:1131–1158
37. Plevako VP (1971) On the theory of elasticity of inhomogeneous media. J Appl Math Mech 35:806–813
38. Reddy JN (2004) Mechanics of laminated composite plates and shells: theory and analysis, 2nd edn. CRC Press, Boca Raton
39. Reddy JN, Cheng ZQ (2001) Three-dimensional thermomechanical deformations of functionally graded rectangular plates. Eur J Mech A/Solids 20:841–855
40. Rosen BW, Hashin Z (1970) Effective thermal expansion coefficients and specific heats of composite materials. Int J Eng Sci 8:157–173
41. Runge C (1901) Über empirische Funktionen und die Interpolation zwischen äquidistanten Ordinaten. Z Math Physik 46:224–243
42. Soldatos KP, Hadjigeorgiou VP (1990) Three-dimensional solution of the free vibration problem of homogeneous isotropic cylindrical shells and panels. J Sound Vibr 137:369–384
43. Tarn JQ, Wang YM (1995) Asymptotic thermoelastic analysis of anisotropic inhomogeneous and laminated plates. J Therm Stress 18:35–58
44. Tornabene F, Fantuzzi N, Viola E, Carrera E (2014) Static analysis of doubly-curved anisotropic shells and panels using CUF approach, differential geometry and differential quadrature method. Compos Struct 107:675–697
45. Tornabene F, Viola E, Fantuzzi N (2013) General higher-order equivalent single layer theory for free vibrations of doubly-curved laminated composite shells and panels. Compos Struct 104:94–117
46. Vel SS (2011) Exact thermoelastic analysis of functionally graded anisotropic hollow cylinders with arbitrary material gradation. Mech Adv Mater Struct 18:14–31
47. Vel SS, Batra RC (2002) Exact solution for thermoelastic deformations of functionally graded thick rectangular plates. AIAA J 40:1421–1433
48. Vel SS, Batra RC (2003) Three-dimensional analysis of transient thermal stresses in functionally graded plates. Int J Solids Struct 40:7181–7196
49. Vlasov BF (1957) On the bending of a rectangular thick plate. Vestnik Moskovskogo Universiteta. Matematika Mekhanika Astronomia N2:25–31
50. Woodward B, Kashtalyan M (2011) Three-dimensional elasticity solution for bending of transversely isotropic functionally graded plates. Eur J Mech A/Solids 30:705–718
51. Wu CP, Chiu KH, Wang YM (2008) A review on the three-dimensional analytical approaches of multilayered and functionally graded piezoelectric plates and shells. Comput Mater Continua 8:93–132